ARL-TR-8749 ● AUG 2019

Trajectory Shaping for Quasi-Equilibrium Glide in Guided Munitions

by Luisa D Fairfax, JD Vasile, Luke S Strohm, and Frank E Fresconi

NOTICES

Disclaimers

The findings in this report are not to be construed as an official Department of the Army position unless so designated by other authorized documents.

Citation of manufacturer's or trade names does not constitute an official endorsement or approval of the use thereof.

Destroy this report when it is no longer needed. Do not return it to the originator.

ARL-TR-8749 ● AUG 2019

Trajectory Shaping for Quasi-Equilibrium Glide in Guided Munitions

by Luisa D Fairfax, JD Vasile, Luke S Strohm, and Frank E Fresconi
Weapons and Materials Research Directorate, CCDC Army Research Laboratory

REPORT DOCUMENTATION PAGE

Form Approved
OMB No. 0704-0188

1. REPORT DATE *(DD-MM-YYYY)*	2. REPORT TYPE	3. DATES COVERED (From - To)
August 2019	Technical Report	1 October 2018–1 July 2019

4. TITLE AND SUBTITLE
Trajectory Shaping for Quasi-Equilibrium Glide in Guided Munitions

5a. CONTRACT NUMBER

5b. GRANT NUMBER

5c. PROGRAM ELEMENT NUMBER

6. AUTHOR(S)
Luisa D Fairfax, JD Vasile, Luke S Strohm, and Frank E Fresconi

5d. PROJECT NUMBER

5e. TASK NUMBER

5f. WORK UNIT NUMBER

7. PERFORMING ORGANIZATION NAME(S) AND ADDRESS(ES)
CCDC Army Research Laboratory
ATTN: FCDD-RLW-LE
Aberdeen Proving Ground, MD 21005

8. PERFORMING ORGANIZATION REPORT NUMBER
ARL-TR-8749

9. SPONSORING/MONITORING AGENCY NAME(S) AND ADDRESS(ES)

10. SPONSOR/MONITOR'S ACRONYM(S)

11. SPONSOR/MONITOR'S REPORT NUMBER(S)

12. DISTRIBUTION/AVAILABILITY STATEMENT
Approved for public release; distribution is unlimited.

13. SUPPLEMENTARY NOTES
ORCID ID: Luke S Strohm, 0000-0002-3303-0041

14. ABSTRACT

The objective of this research is to extend range, increase impact velocity, decrease time-of-flight, and reduce spikes in thermal loading in long-range munitions. This is done by commanding munitions to quasi-equilibrium glide at an optimum height, which cancels out the phugoid motion. The phugoid motion is a longitudinal oscillatory mode in which the munition first pitches up as it climbs and slows in speed followed by pitching down and speeding up at a near-constant angle-of-attack. It is more pronounced in long-range flights in which the air density is lower at atmosphere, allowing the munition to reach higher altitudes before slowing down. Quasi-equilibrium glide is adapted from space entry vehicles and is typically used to reduce heating effects of entry into the atmosphere. Thermal loads and temperature effects are also explained. Monte Carlo simulations are shown on an example munition for maximal range and terminal guidance scenarios. Trajectory shaping is also used for imperfectly located targets. A worst-case scenario is shown in which the target is imperfectly located at launch. In this case, impact velocity is improved by 56.5%, and range error is decreased by 86.8% in a long-range guidance scenario to 250 km. This report is organized as follows: first, the introduction outlines past work regarding munition characterization and control and the phugoid motion control; second, the governing equations are outlined; third, GENEX and the baseline gliding and terminal guidance are outlined followed by the maximum glide height, trajectory shaping, evaluation, maximal range results, terminal guidance, and a conclusion.

15. SUBJECT TERMS
trajectory shaping, guidance, flight control, long-range munitions, projectile, maneuver, flight theory, phugoid

16. SECURITY CLASSIFICATION OF:			17. LIMITATION OF ABSTRACT	18. NUMBER OF PAGES	19a. NAME OF RESPONSIBLE PERSON
a. REPORT	b. ABSTRACT	c. THIS PAGE			Luisa D Fairfax
Unclassified	Unclassified	Unclassified	UU	32	19b. TELEPHONE NUMBER (Include area code) (410) 306-2104

Contents

List of Figures

List of Tables

1. Introduction

Past work has focused on guided munition dynamic modeling and control at lower altitude, with constant atmospheric conditions. Some guided munitions are limited in control authority. As a result, existing control methods use the munition flight dynamics to nudge the munition throughout flight toward a target, azimuth angle, impact velocity, or maximal range (Fresconi 2011; Fresconi et al. 2015). The impact point predictor (Cooper et al. 2012) solves for time-to-go by assuming constant aerodynamic and atmospheric conditions. It then calculates a ballistic estimate of the impact point to determine the best time to transition from gliding to terminal guidance. For terminal guidance, the Generalized Vector Explicit Guidance (GENEX) law has been developed. GENEX improves miss distance by customizing design cost functions (Ohlmeyer and Phillips 2006) to balance miss distance against impact angle requirements.

Past work has also eliminated phugoid oscillations in shuttle and other entry vehicles (Lu et al. 2013; Lu 2014). An equilibrium glide command is performed based on the first-order solution of the vertical plane motion for reentry. Eliminating the trajectory oscillations successfully decreased the heating rate, load factor, and dynamic pressure, which would spike due to the trajectory oscillation motion. Existing literature does not discuss quasi-equilibrium glide or damping the phugoid in high-altitude flight for guided munitions.

The goal of this report is to develop quasi-equilibrium glide commands in the guided munitions to smooth dynamic loading and heating conditions and to improve target miss distance. Additionally, quasi-equilibrium glide commands alter the time-of-fight to enable multiple munitions to be shot out of the same gun with the same arrival time. The change in atmospheric conditions and reduced air density cause the phugoid oscillations. The maximum altitude at which sufficient control authority exists for equilibrium glide is calculated. The contribution of this report is a guided munition glide and terminal guidance algorithm that smooths heating and dynamic loading, reduces miss distance, and enables multiple rounds to be delivered simultaneously to the target from the same gun. The report is organized as follows: in Section 2, the governing equations are introduced; in Section 3, the GENEX baseline glide and terminal guidance algorithm is discussed. Section 4 discusses the maximum glide height. Section 5 details trajectory shaping. The evaluation is in Section 6, and Section 7 concludes the report.

2. Governing Equations

The munition dynamics are modeled using the point mass model (Fresconi 2011; McCoy 2012; Fresconi et al. 2015). The states are positions and velocities oriented north (toward the target), east and down as shown:

$$X = [x,\ y,\ z,\ \dot{x}\ ,\ \dot{y},\ \dot{z}]^T. \tag{1}$$

The spherical earth model is used, and z is then the height minus the earth's radius. The point mass dynamic equations are as shown in Eqs. 2–5,

$$C_{\hat{D}} = \frac{1}{8m}\rho\pi D^2 C_D, \tag{2}$$

$$\ddot{x} = -C_{\hat{D}}\, V\dot{x} + \frac{L_x+T_x}{m} - \vec{g} + 2\vec{v}_T \times \vec{\omega}_E, \tag{3}$$

$$\ddot{y} = -C_{\hat{D}} V\ \dot{y} + \frac{L_y+T_y}{m} - \vec{g} + 2\vec{v}_T \times \vec{\omega}_E, \tag{4}$$

$$\ddot{z} = \ -C_{\hat{D}}\, V\dot{z} + \frac{L_z+T_z}{m} - \vec{g} + 2\vec{v}_T \times \vec{\omega}_E, \tag{5}$$

where C_D is the aerodynamic drag coefficient, V is the total munition velocity, m is the munition mass, D is the munition diameter, ρ is the atmospheric pressure, L_i is the lift in the i = x, y, z directions, T_i is the thrust in the i = x, y, z directions, $\vec{g}$ is the acceleration due to gravity, $v_T = [\dot{x} \quad \dot{y} \quad \dot{z}]^T$, and $\vec{\omega}_E$ is the Earth's rotation rate. A spherical earth model is used. The 1976 standard atmosphere array is used.

A simplified theoretical analysis was employed to estimate the aerodynamic heating of the munition during flight. As derived by Allen and Eggers (1953), and outlined by Jerger (1960) and Fleeman (2012), the heat transfer coefficient for a given nose tip bluntness at stagnation and temperature gradient at the nose were computed using Eqs. 6–13. The analysis assumes 1-D conduction heat transfer, a laminar boundary layer at the nose, stagnation heating, and negligible radiation.

$$T_{R_{stag}} = T_0\left(1 + \frac{\gamma-1}{2}M^2\right), \gamma = 1.4, \tag{6}$$

$$\mu_{air_{stag}} = 1.147 \times 10^{-6}\left(\frac{708}{\left(T_{R_{stag}}+216\right)} \cdot \left(\frac{T_{R_{stag}}}{492}\right)^{3/2}\right), \tag{7}$$

$$k_{air_{stag}} = 3.58 \times 10^{-6}\left(\frac{717}{\left(T_{R_{stag}}+225\right)} \cdot \left(\frac{T_{R_{stag}}}{492}\right)^{3/2}\right), \tag{8}$$

$$P_r = \frac{c_p \cdot \mu_{air_{stag}}}{k_{air_{stag}}}, \tag{9}$$

$$Re_{d_{Nose}} = \frac{\rho_0 V_0 d_{Nose}}{\mu_{air_{stag}}}, \tag{10}$$

$$N_{NU} = 1.321 \cdot Re_{d_{Nose}}{}^{0.5} \cdot P_r{}^{0.4}, \tag{11}$$

$$h_r = N_{NU} \cdot \frac{k_{air_{stag}}}{d_{Nose}}, \tag{12}$$

$$\frac{dT}{dt} = \frac{h_r \cdot \left(T_{R_{stag}} - T_0\right)}{c_{struct} \cdot \rho_{struct} \cdot z_{struct}}, \tag{13}$$

where $T_{R_{stag}}$ (°R) is the stagnation recovery temperature, or the temperature of the boundary layer at the nose surface, and T_0 is the temperature at sea level. $\mu_{air_{stag}}$ (lb/s·ft) is the viscosity of the air at the nose surface. $k_{air_{stag}}$ (BTU/s·ft·°R) is the conductivity of the air at the nose surface. P_r is the Prandtl number, where c_p (BTU/lb·°R) is the constant specific heat of air. $Re_{d_{Nose}}$ is the Reynolds number based on the nose tip diameter, d_{Nose} (ft), ρ_0 is the freestream air density, and V_0 is the freestream velocity. As derived by Allen and Eggers (1953), N_{NU} is the Nusselt number of a laminar boundary layer over a blunt nose, and h_r (BTU/ft^2·s·°R) is the convection heat transfer coefficient of a blunt nose. The temperature gradient at the nose, $\frac{dT}{dt}$, is estimated based on the specific heat, c_{struct} (BTU/lb·°R), density, ρ_{struct}(lb/ft^3), and thickness, z_{struct} (ft), of the airframe structure, respectively.

The temperature of the nose can be estimated based on the prediction of the heat transfer coefficient throughout flight. The heat transfer coefficient at the nose is updated throughout the flight trajectory and is used to compute the temperature gradient. An aluminum alloy skin without external insulation of 0.2 inches was used for the airframe structure. The aluminum skin was modeled as a thermally thin surface, exhibiting high heat transfer, where the temperature is constant through the thickness of the surface. The temperature gradient (Eq. 13) is based on the method from Jerger (1960) for a thermally thin airframe structure with "nearly perfect" insulation behind the airframe (i.e., adiabatic wall). The radiation from the airframe surface is also assumed negligible (Allen and Eggers 1953; Jerger 1960; Hale 1994; Fleeman 2012).

3. GENEX: Baseline Glide and Terminal Guidance

The baseline guidance commands are earth-fixed GENEX commands (Ohlmeyer and Phillips 2006). The munition is an indirect fire and is shot ballistically. At apogee, the munition is commanded to glide. The traditional gliding commands use GENEX and are given in earth acceleration x, y, z and are later transformed into

the body frame (Fresconi 2011). The earth-fixed GENEX commands are explained in detail by Ohlmeyer and Phillips (2006) and are also shown in Eqs. 14–27. The guidance is based on the difference between the target and the munition position and velocity.

$$r_x = x_T - x, \tag{14}$$

$$r_y = y_T - y, \tag{15}$$

$$r_z = z_T - z, \tag{16}$$

$$\dot{r}_x = \dot{x}_T - \dot{x}, \tag{17}$$

$$\dot{r}_y = \dot{y}_T - \dot{y}, \tag{18}$$

$$\dot{r}_z = \dot{z}_T - \dot{z}, \tag{19}$$

where the target position and velocity states in the earth frame are $\begin{bmatrix} x_T & y_T & z_T & \dot{x}_T & \dot{y}_T & \dot{z}_T \end{bmatrix}^T$. The resulting radii are calculated and guidance gains are calculated,

$$r_{xyz} = \sqrt{r_x^2 + r_y^2 + r_z^2}, \tag{20}$$

$$\dot{r}_{xyz} = \frac{r_x \dot{r}_x + r_y \dot{r}_y + r_z \dot{r}_z}{r_{xyz}}, \tag{21}$$

$$K_1 = (n+2)(n+3), \tag{22}$$

$$K_2 = -(n+1)(n+2), \tag{23}$$

where n is the desired cost function guidance gain (and is set to 0 in this analysis). The normalized velocity, v, desired final velocity vector, v_F, and normalized radius, r, are computed as shown,

$$v = \frac{[\dot{x} \quad \dot{y} \quad \dot{z}]}{|\dot{r}_{xyz}|}, \tag{24}$$

$$v_F = -\frac{[1/\tan(AOF) \quad 0 \quad 1]}{\sqrt{\left(\frac{1}{\tan(\mathrm{AOF})}\right)^2 + 1,}} \tag{25}$$

$$r = \frac{[r_x \quad r_y \quad r_z]}{r_{xyz}}, \tag{26}$$

where AOF is the desired angle-of-fall in radians. The command in earth coordinates is then as shown,

$$u = -\left(\frac{-(\dot{r}_{xyz})^2}{r_{xyz}}(K_1(r-v) + K_2(v-v_F))\right), \tag{27}$$

$$a_{xe} = u(1), \tag{28}$$

$$a_{ye} = u(2), \tag{29}$$

$$a_{ze} = u(3) - g. \tag{30}$$

The command is converted into munition body coordinates using the transformation matrix T_{E2V}. The final body commands, $[a_{xv} \quad a_{yv} \quad a_{zv}]^T$, are only applied to the axial and vertical axes,

$$L = T_{E2V}\begin{bmatrix} a_{xe} \\ a_{ye} \\ a_{ze} \end{bmatrix}. \tag{31}$$

For GENEX glide commands the focus is to have a large gain on the vertical up direction in order to extend range. GENEX glide commands are used to ensure cross range is kept to a minimum. The x command is left uncontrolled in order to maximize downrange,

$$\begin{bmatrix} a_{xv} \\ a_{yv} \\ a_{zv} \end{bmatrix} = \begin{bmatrix} 0 \\ L(2) \\ L(3) \end{bmatrix}. \tag{32}$$

And for guide-to-hit terminal commands, the x command is based on the target location and is as shown,

$$\begin{bmatrix} a_{xv} \\ a_{yv} \\ a_{zv} \end{bmatrix} = L. \tag{33}$$

4. Maximum Glide Height

The reason for the trajectory oscillations is the change in atmosphere at higher altitudes. The change in atmosphere affects the munition's control, and at higher altitudes, there is less air to provide lift to the control surfaces. The munition will therefore be unable to perform a quasi-equilibrium glide above a certain altitude. The maximum glide height is calculated by balancing the forces on the munition as illustrated in Fig. 1 and as shown in Eq. 34,

$$W + D_F \sin\theta \geq L\cos\theta, \tag{34}$$

$$mg + \frac{1}{2}\frac{\pi}{4}\rho V^2 D^2 C_D \sin\theta \geq \frac{1}{2}\frac{\pi}{4}\rho V^2 D^2 C_L \cos\theta, \quad (35)$$

where θ is the pitch angle, D is the diameter, C_D is the drag coefficient, C_L is the lift coefficient, and ρ is the air density. The air density is solved for and used to calculate the maximum glide height in the atmospheric model look-up table. Next, the trajectory-shaping command necessary to glide at the maximum glide height is explained.

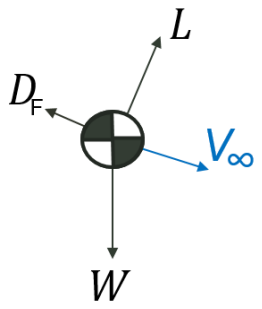

Fig. 1 Munition free body diagram where L is the lift, D_F is drag force, V is the total free stream velocity, and W is weight. The lift is required to be sufficient such that the munition can sustain semi-level flight.

5. Trajectory Shaping

The trajectory shaping was first developed for quasi-equilibrium glide in entry vehicles (Lu 2014). The flight path angle, γ, is defined using a spherical earth model

$$\dot{r} = V \sin\gamma, \quad (36)$$

in which $\dot{r}$ is the change in radius from the Earth's center. The desired glide flight path angle, γ_{QEGC}, is calculated as shown and is fed into the desired altitude rate, $\dot{h}_{QEGC}$. The desired altitude rate is then used to calculate the desired command in the z direction, a_{ze},

$$\gamma_{QEGC} = \frac{(V^2 + L)}{\frac{V^2}{2}\mathrm{B}_r\left(\frac{C_D}{C_L}\right)}, \quad (37)$$

$$\dot{h}_{QEGC} = V \sin\gamma_{QEGC}, \quad (38)$$

$$a_{ze} = L - k(\dot{h} - \dot{h}_{QEGC}), \quad (39)$$

where $\left(\frac{\partial\rho}{\partial r}\right)/\rho = \mathrm{B}_r \approx -900$ and the equatorial radius of the Earth is $R_0 = 6{,}378{,}135\ m$, L is the lift, $k = 20$ is the gain, and C_D and C_L are the drag and lift coefficients.

6. Evaluation

Evaluation was performed on a long-range munition (Strohm 2019). The example munition parameters are shown in Table 1. Two cases were run. The first case was run for maximum range, and the second case was a guide-to-hit for a target located at 130 km. Two trajectory-shaping guidance methods were evaluated along with the baseline GENEX glide, and all methods used GENEX as the guide-to-hit terminal guidance. Trajectory shaping needed to be commanded within a percentage of the optimum glide height to ensure that the munition achieved the optimum glide height. Both trajectory-shaping glide commands were triggered at 65% of the glide height. The 65% decision was developed from a sensitivity study (not shown) for maximum range. The trade-off was made between flying in at higher altitude, which is good for range, and gaining controllability earlier, which is also good for range. In pre-apogee trajectory shaping, glide was allowed to occur anytime from the beginning of flight once the minimum height was reached. For post-apogee trajectory shaping, trajectory shaping could occur after apogee while vertical acceleration was upward. This is because once the munition is uncontrollable at a high altitude, the munition will come down below the optimum glide height. It will then be commanded to fly up to the optimum glide height. Initial conditions were optimized for either max range or guide-to-hit using Newton's method. The optimization is not unique as the problem is not concave. The optimization results yielded a quadrant elevation (QE) of 65° for guide-to-hit with a target at 130 km. For maximal range, the QE was 54° for baseline and for post-apogee trajectory shaping. For pre-apogee trajectory shaping, the QE was 61.8°.

Table 1 Long-range precision fires tactical parameters

Parameter	Value
Munition diameter (mm)	105
Munition length (m)	1.05
Initial flight mass (kg)	27.3114
Muzzle velocity (m/s)	1,416.2
QE (degrees)	70.0
Rocket engine start time (s)	10
Rocket engine total burn time (s)	7.7681
Rocket engine first stage thrust (N)	559.2

6.1 Maximal Range Results

Example results are as shown in Fig. 2. For comparison, the baseline gliding for maximal range trajectory (GENEX) is shown. Trajectory oscillation-cancellation is shown at various altitudes. The varying ranges due to gliding altitude show that atmospheric density affects maximal downrange performance. Trajectory oscillation reduction maneuvers begin at altitude in order to increase range. The trajectory oscillation motion occurs because the munition cannot control at too high of an altitude and begins to a motion in which it bounces off of the atmosphere and back into a lower atmosphere. An equilibrium glide is commanded at 20,000 m based on the free-body diagram. The highest equilibrium glide possible produced the greatest range. A Monte Carlo of 100 simulations was run with varying aerodynamic tables and initial conditions as shown in Table 2.

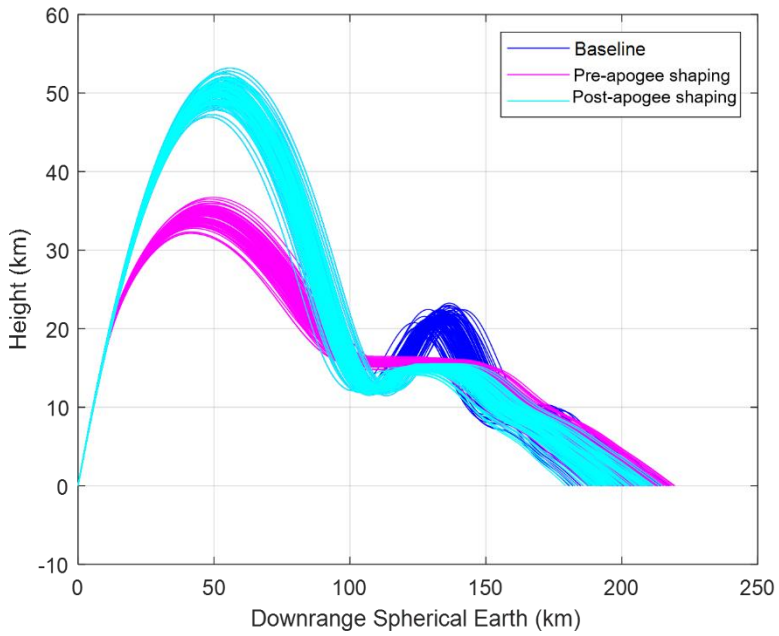

Fig. 2 Height vs. downrange spherical earth. Demonstrates equivalent maximum range among trajectory shaping and baseline GENEX gliding maneuvers.

Table 2 Monte Carlo simulation uncertainty parameters 1 standard deviation

Parameter	Uncertainty
Velocity (m/s)	3
Pointing angle error (degrees)	0.28125
Atmospheric density (%)	0.5
Wind (m/s)	10
Aerodynamic (%)	3
Engine (%)	2
Thrust misalignment (degrees)	0.1

The results are plotted on top of each other in Fig. 2. The baseline uses GENEX glide commands starting at apogee. Pre-apogee trajectory shaping begins to adjust the trajectory into equilibrium glide at optimum glide height beginning at 65% of optimum glide height. Post-apogee trajectory shaping adjusts the trajectory to equilibrium glide beginning at 65% of optimum glide height beginning after apogee. Trajectory shaping reduces time-to-range. Figure 3 shows that jumps in velocity are reduced using trajectory shaping. Impact velocity for max range glide is about the same. The increase in velocity at 10 s is due to the rocket motor being turned on. Figure 4 shows the dynamic pressure. Dynamic pressure loading is decreased with pre-apogee trajectory shaping, that is turning the control on before apogee, when the control is typically turned on. Figure 5 shows the effect of the heat transfer coefficient and its integral to show the effect of heat transfer over time. Stress points decrease with trajectory shaping. At first, the area under the curve is higher due to flying in denser atmosphere, but the final area under the curve is equivalent due to lower time-of-flight in trajectory-shaped flights. Figure 6 shows the heat flux. In order to reduce heat flux at the first skip into the atmosphere, the shaping needs to begin before the first apogee. Figure 7 shows the temperature at the nose. The temperature at the nose is initially higher with trajectory shaping due to flying at denser atmosphere. By the end of flight, temperature decreases and could be beneficial for longer flights to reduce heating. Figure 8 shows the downrange dispersion for maximal glide commands. The maximal downrange is similar for trajectory shaping and baseline methods. Finally, impact velocity for maximal glide is shown in Fig. 9. Impact velocity for maximal glide is equivalent. Next, the terminal guidance results will be shown.

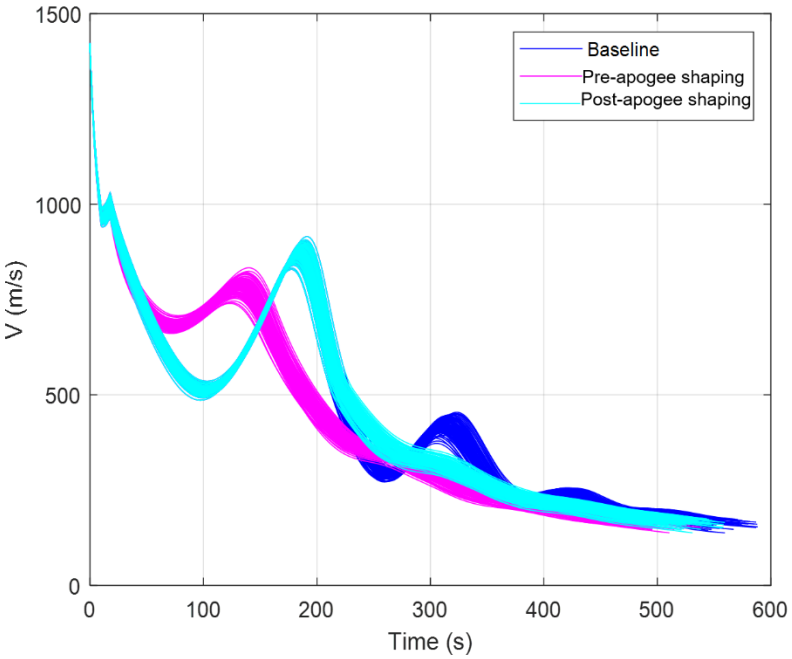

Fig. 3 Gliding velocity is equivalent among gliding trajectories

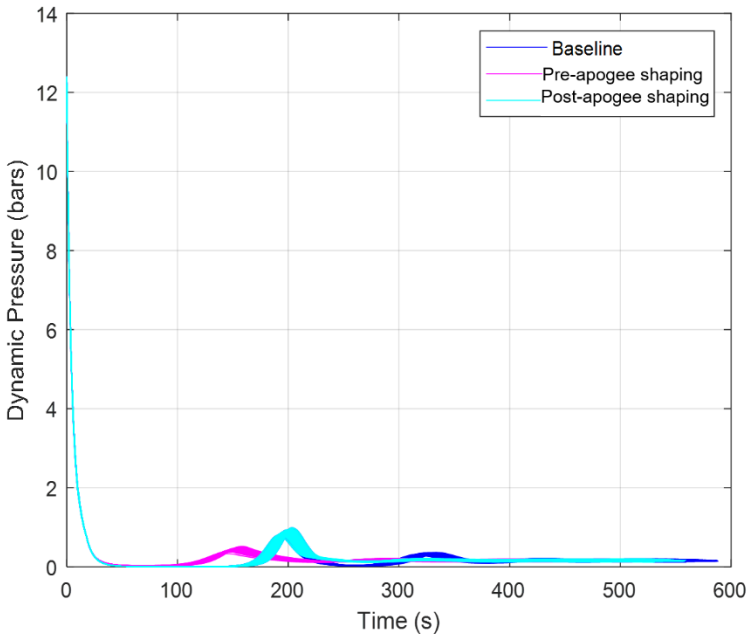

Fig. 4 Gliding dynamic pressure

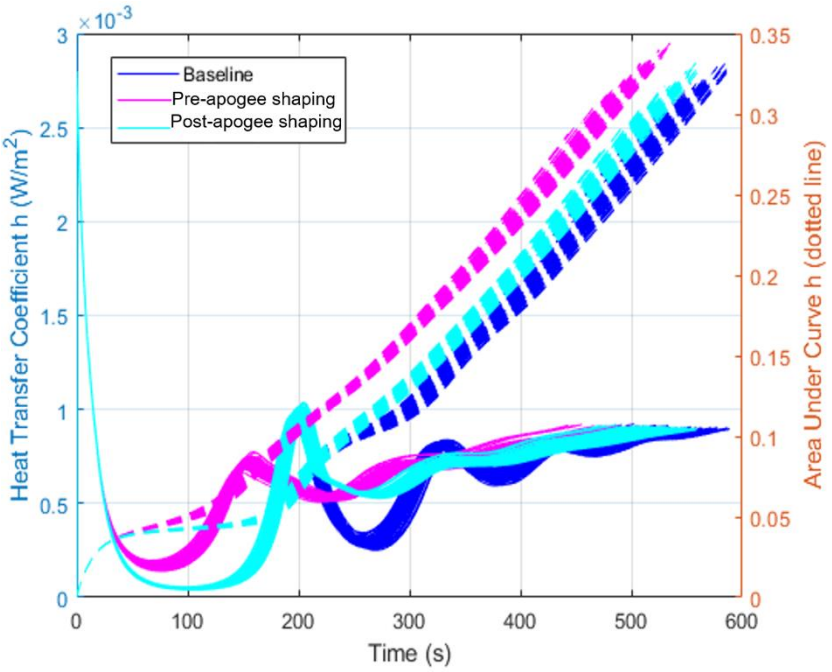

Fig. 5 Gliding heat transfer coefficient and area under the curve

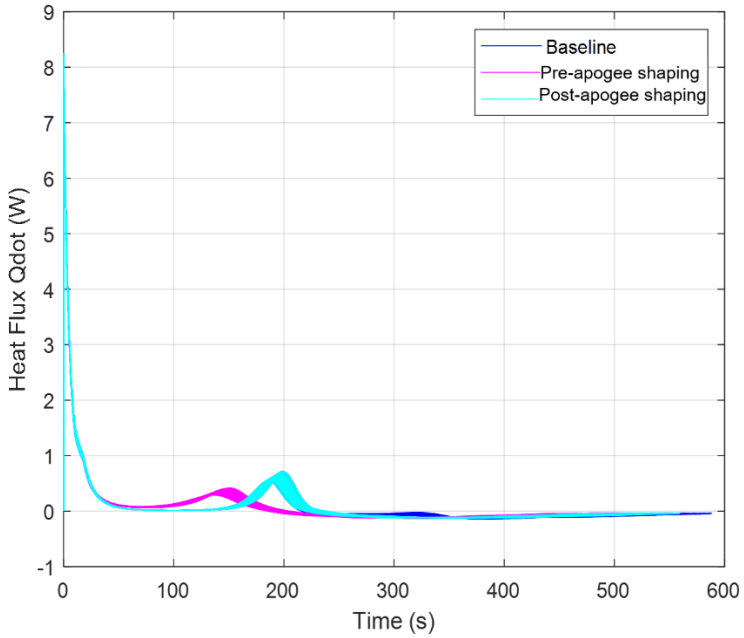

Fig. 6 Gliding heat flux

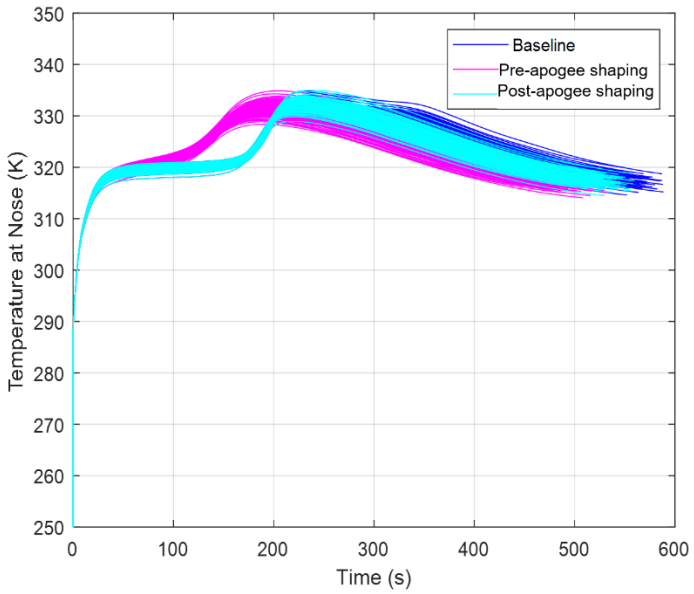

Fig. 7 Temperature at the nose where the initial temperature, T_0, is 288.15 K in accordance with the 1976 Standard Atmosphere model

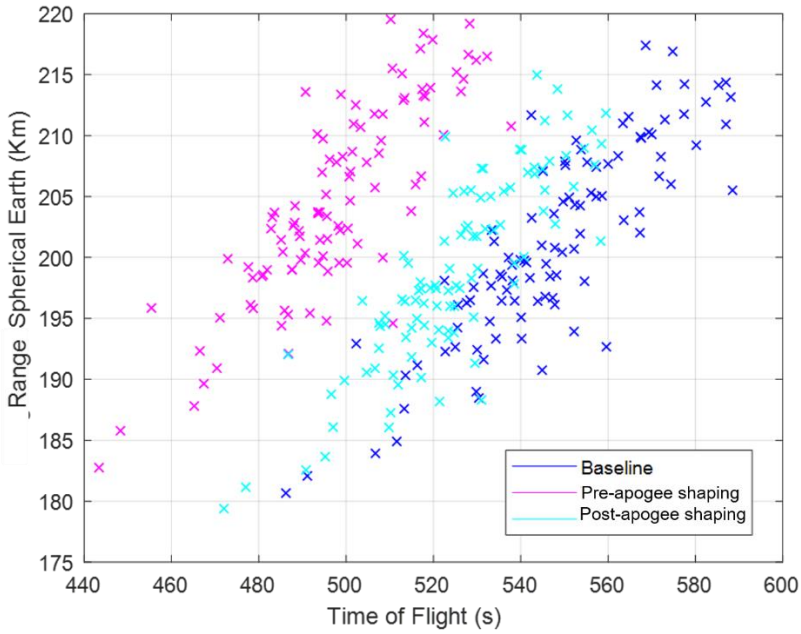

Fig. 8 Downrange for maximal glide commands

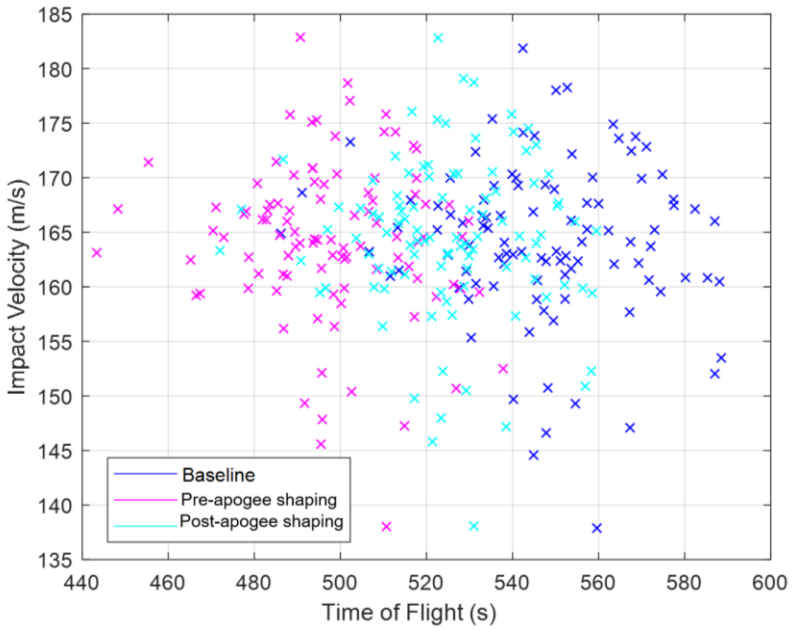

Fig. 9 Impact velocity. Maximizing for downrange produces similar impact velocity.

6.2 Terminal Guidance

Two terminal guidance scenarios were run. In the first scenario, the target was placed at 130 km, and in the second scenario, a 30% rocket was available. The transition to endgame is based on a modified version of the impact point predictor. The impact point predictor (Fresconi et al. 2015) uses the closed-form aerodynamic equations, which assume a ballistic flight with constant atmospheric and drag conditions. At high altitude, constant assumptions are violated, making the standard impact point predictor unable to determine the best time to transition to endgame. In order to enforce the closed-form constraints, an additional requirement is placed on the impact point predictor. A heuristically determined range requirement was added in order to ensure that the impact point predictor closed-form solution assumptions are met.

$$|x_T - x| < \frac{x_T}{8}, \tag{40}$$

where x_T is the target downrange and x is the munition downrange. The desired terminal angle of fall is set to 80° in order to increase terminal effects. In pre-apogee trajectory shaping, the munition maximum height is decreased. This allows the munition to gain control sooner and not be required to go as low in the atmosphere at the first perigee. The result is more control to enable a quasi-equilibrium glide at a higher optimum atmosphere. Figure 10 shows the height versus downrange spherical earth for the worst-case scenario in which the target is placed in a position

of the phugoid that is unreachable using the baseline glide method. The baseline uses GENEX glide commands starting at apogee. A pre-apogee trajectory-shaping command begins to shape the trajectory into equilibrium glide at optimum glide height beginning at 65% of optimum glide height. A post-apogee trajectory-shaping command shapes the trajectory to equilibrium glide beginning at 65% of optimum glide height beginning after apogee. Figure 11 shows the velocity. Jumps in velocity are reduced using trajectory shaping. The final impact velocity is the same. The increase in velocity at 10 s is due to the rocket motor being turned on. Figure 12 shows the dynamic pressure. Dynamic pressure loading is decreased with pre-apogee trajectory shaping, in which trajectory shaping is turned on immediately. Figure 13 shows the heat transfer coefficient. The maximal heat transfer is less with trajectory shaping. The final area under the curve is slightly less using pre-apogee trajectory shaping. Note the change in time-of-flight from pre-apogee trajectory shaping compared with the baseline. Figure 14 shows the heat flux over time-of-flight. In order to reduce heat flux at the first skip into the atmosphere, the shaping needs to begin before the first apogee with the same trend as in the maximal range plot. Temperature at the nose is shown in Figure 15. Temperature at the nose is initially higher with trajectory shaping due to flying at a denser atmosphere and a faster time-of-flight. Figure 16 shows range error. Trajectory shaping, especially pre-apogee trajectory shaping, significantly decreases the dispersion. Figure 17 shows the impact velocity. Impact velocities are similar and slightly higher in the baseline, although the baseline frequently missed the target. There is a significant difference in time-of-flight based on glide method. This could allow multiple munitions to be shot from the same gun.

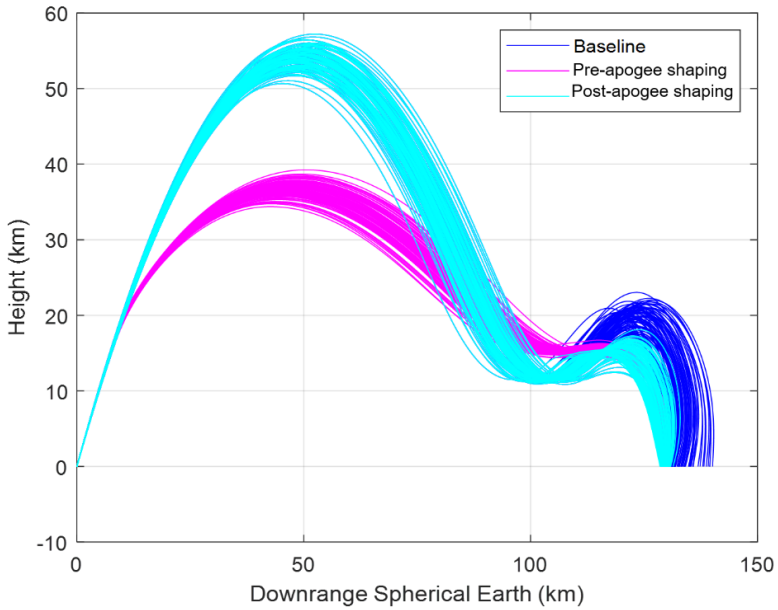

Fig. 10 Height vs. downrange spherical earth for worst-case terminal guidance

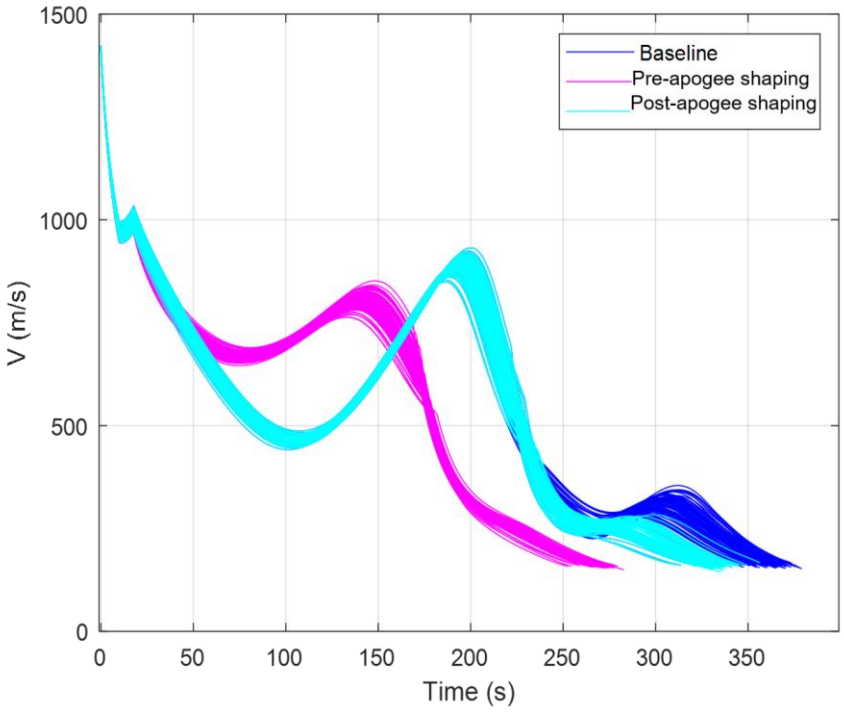

Fig. 11 Velocity

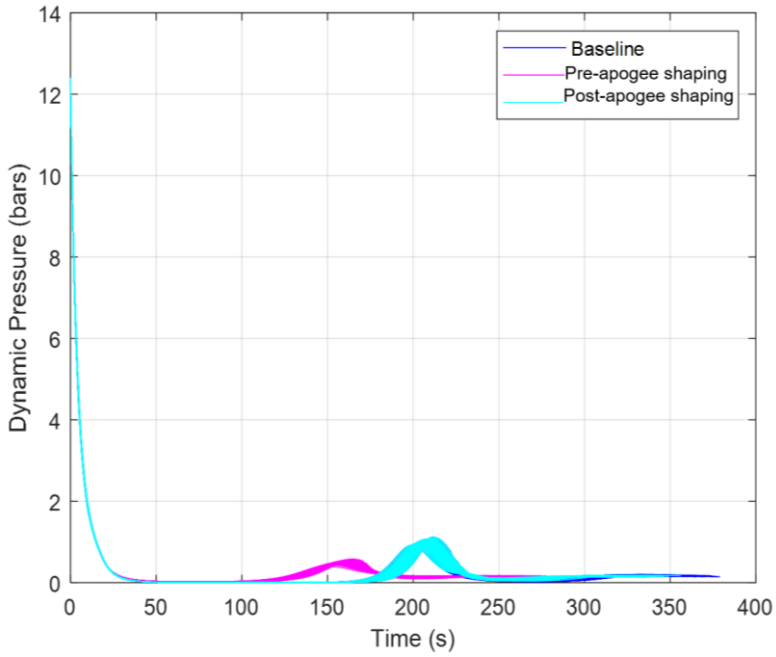

Fig. 12 Terminal guidance dynamic pressure

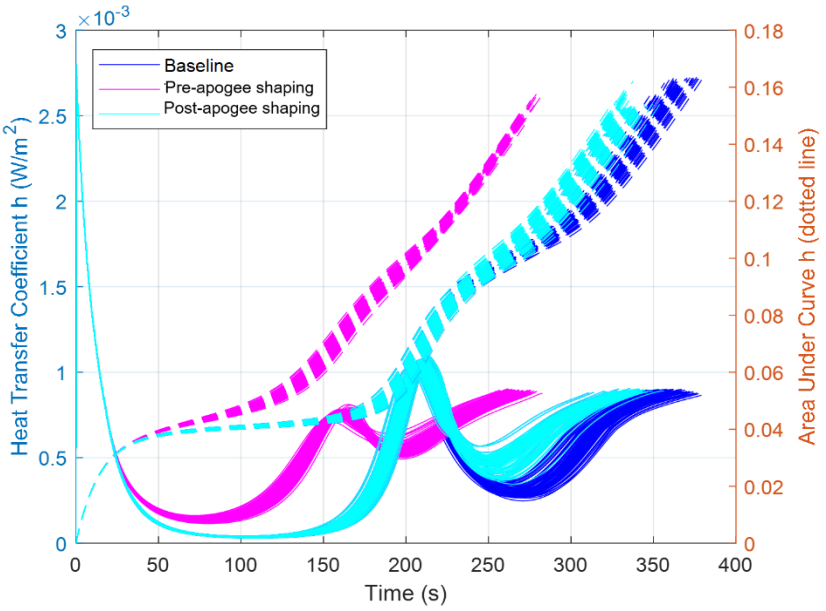

Fig. 13 Heat transfer coefficient

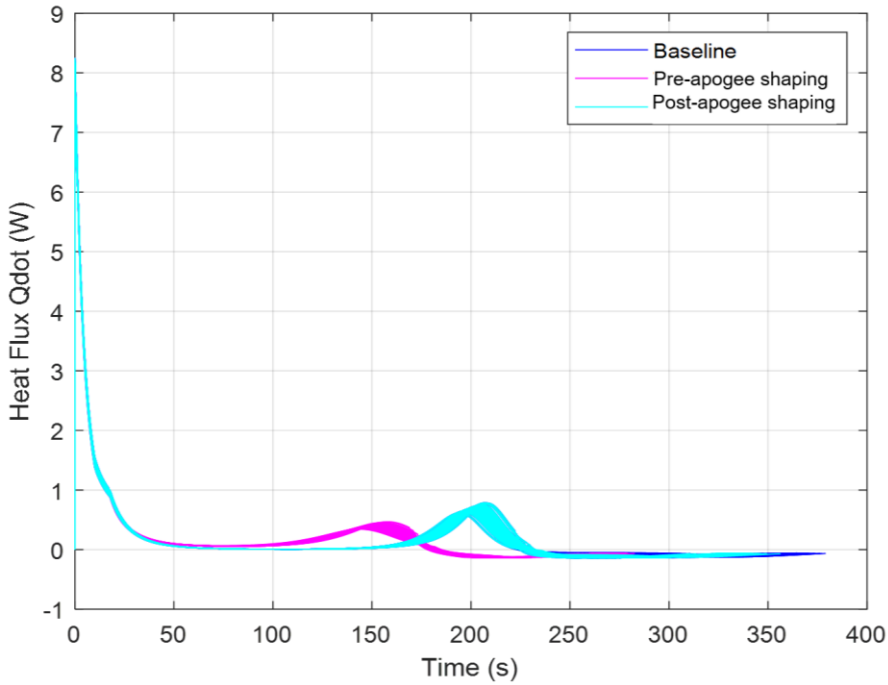

Fig. 14 Terminal guidance heat flux

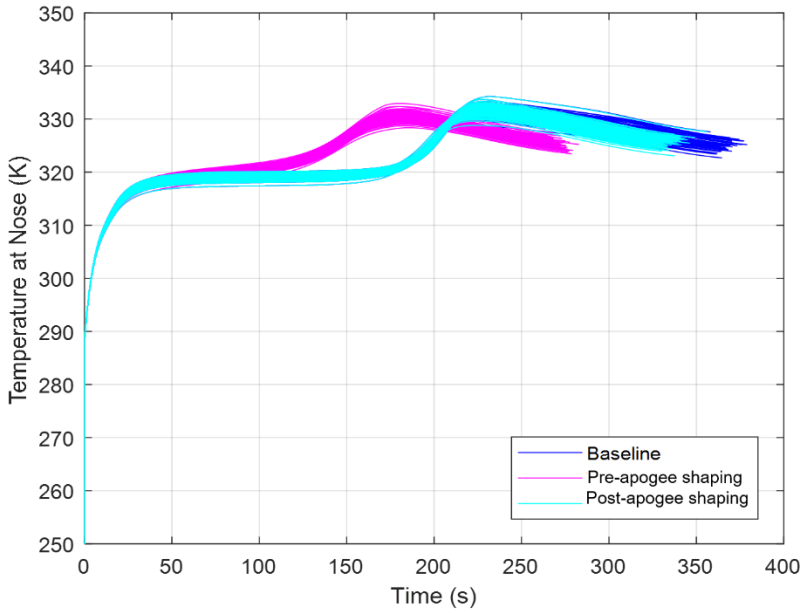

Fig. 15 Temperature at the nose

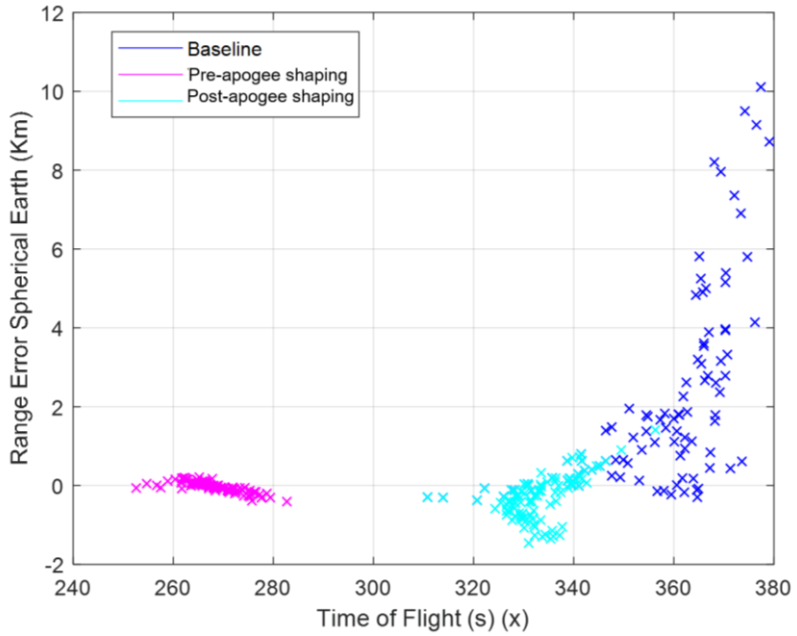

Fig. 16 Downrange error from target in kilometers

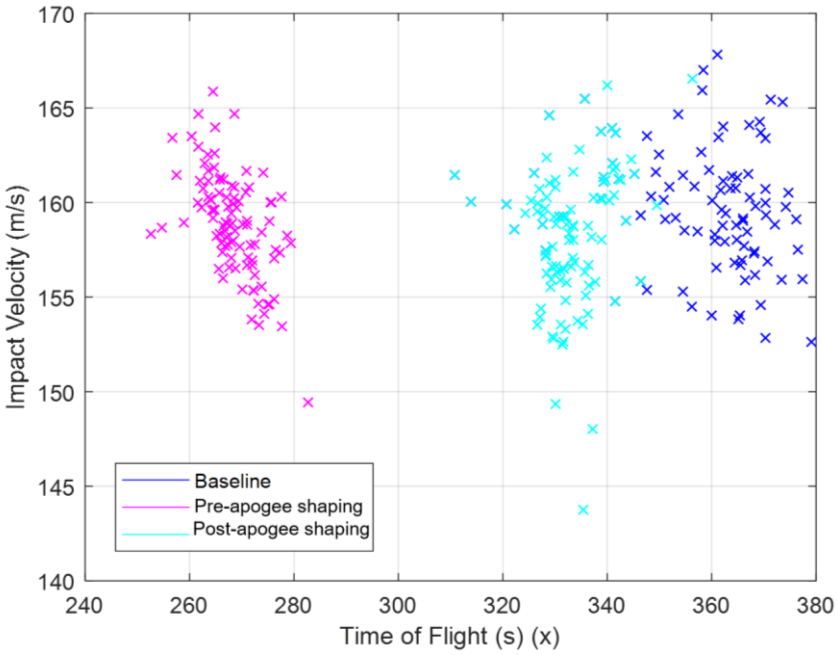

Fig. 17 Impact velocity

In the next scenario, the rocket motor is increased to 50%, and the target is placed at 300 km. The purpose of this trajectory is to show the capabilities of the trajectory shaping with a target up to 300 km. Higher speed and longer time-of-flight conclusions could be different, and the purpose of this report is to show the capabilities of trajectory shaping. Baseline and pre-apogee trajectory shaping scenarios are run. In this flight, only 1 phugoid oscillation had time to take place. As a result, post-apogee trajectory shaping did not have time to diverge from the baseline, so it is omitted. In a longer flight with multiple oscillations, the post-apogee trajectory shaping would diverge from the baseline. Figure 18 shows the munition height versus downrange trajectory, which shows an equilibrium glide at about 20 km. This enables gliding at a higher atmosphere. The result is that the munition does not fall short, can have a steeper angle of descent, and has an increased impact velocity. Figure 19 shows velocity over time-of-flight. Figure 20 shows the dynamic pressure. The dynamic pressure is increased due to less time at very high altitudes, in which the low air density lowers the dynamic pressure. Figure 21 shows the heat transfer coefficient and area under the curve are comparable with and without trajectory shaping. However, the lower time-of-flight can reduce the area under the curve despite the increase in heat transfer coefficient at the end of flight. Figure 22 shows heat flux. The heat flux is highest at launch for both trajectories. The most stressful time in flight is at the lowest atmospheric point. Because the trajectory-shaped munition does not reach as low of an atmosphere, the heat flux peak (around 200 s) is lower. Figure 23 shows temperature at the nose.

The temperature at the nose is comparable between the baseline and shaped trajectories. The shaped trajectories sometimes have a higher temperature due to spending more time at a lower atmosphere (higher air density). The main contribution to temperature at the nose are velocity and height (or air density).

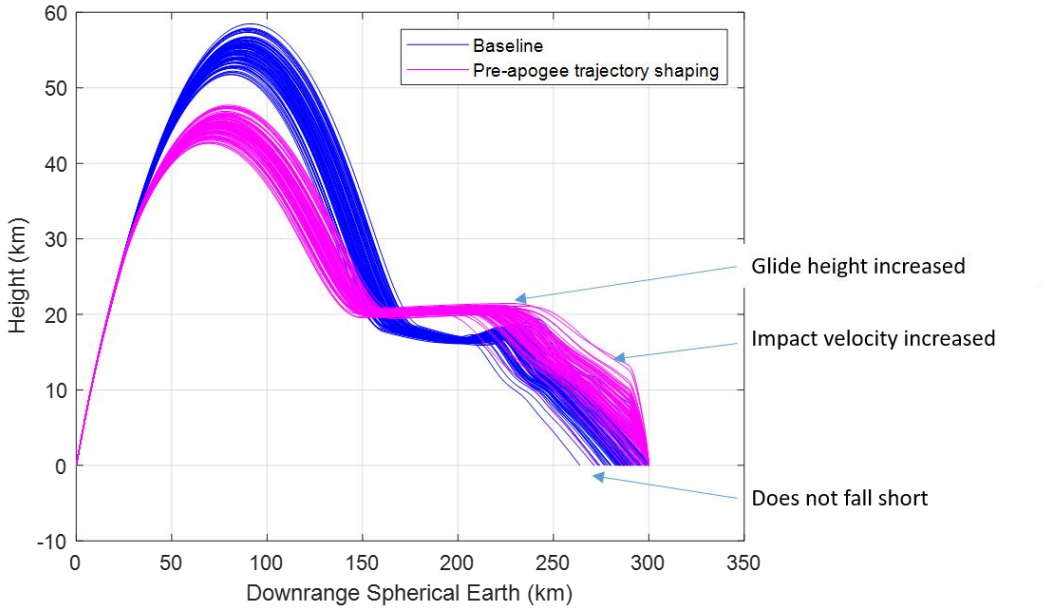

Fig. 18 Munition height vs. downrange trajectory shows an equilibrium glide at about 20 km

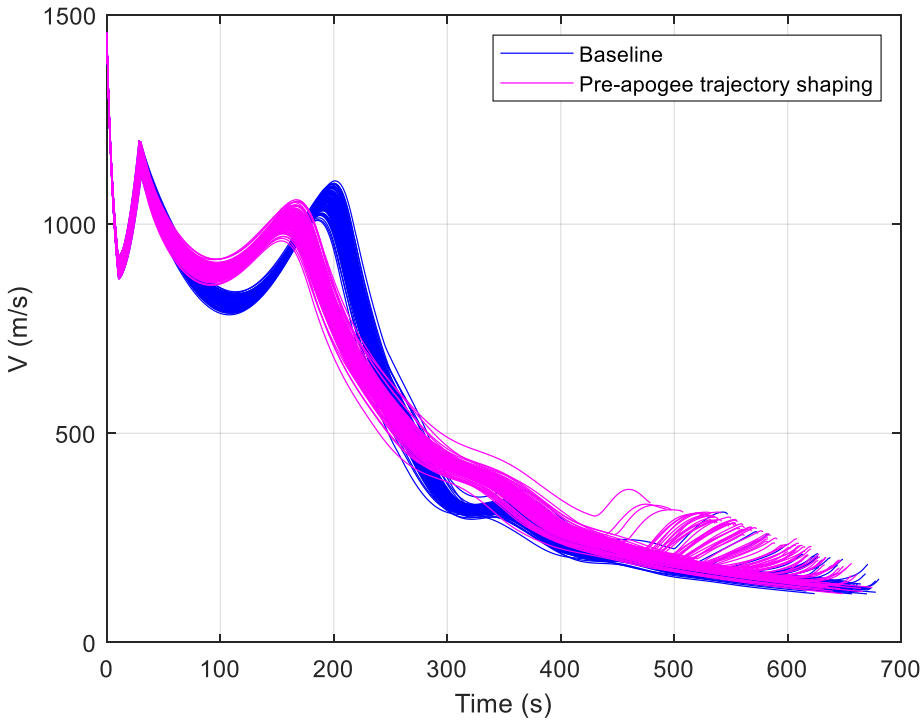

Fig. 19 Velocity over time-of-flight shows a similar decrease in velocity over time

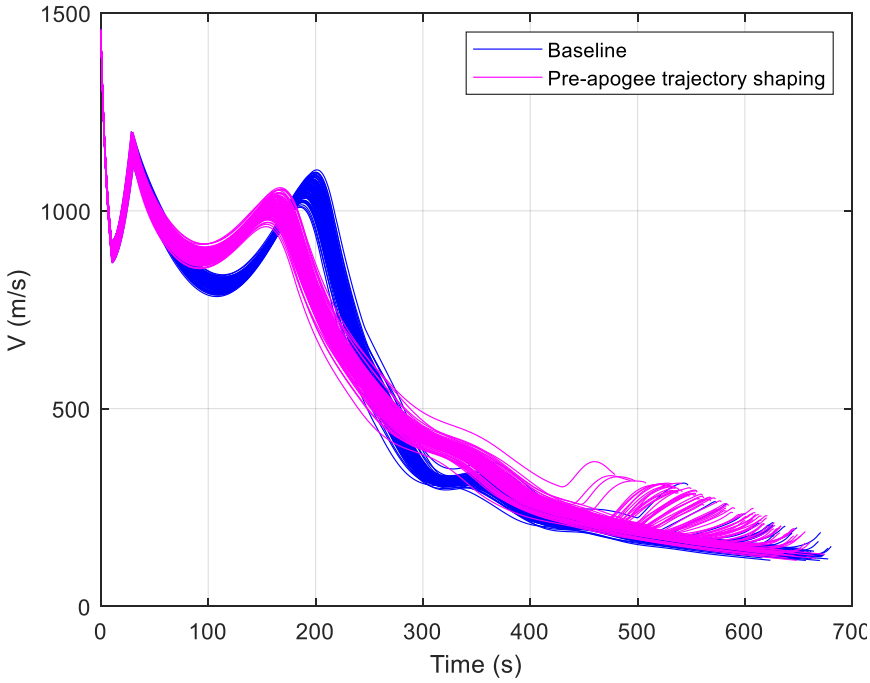

Fig. 20 Increased rocket motor terminal guidance dynamic pressure

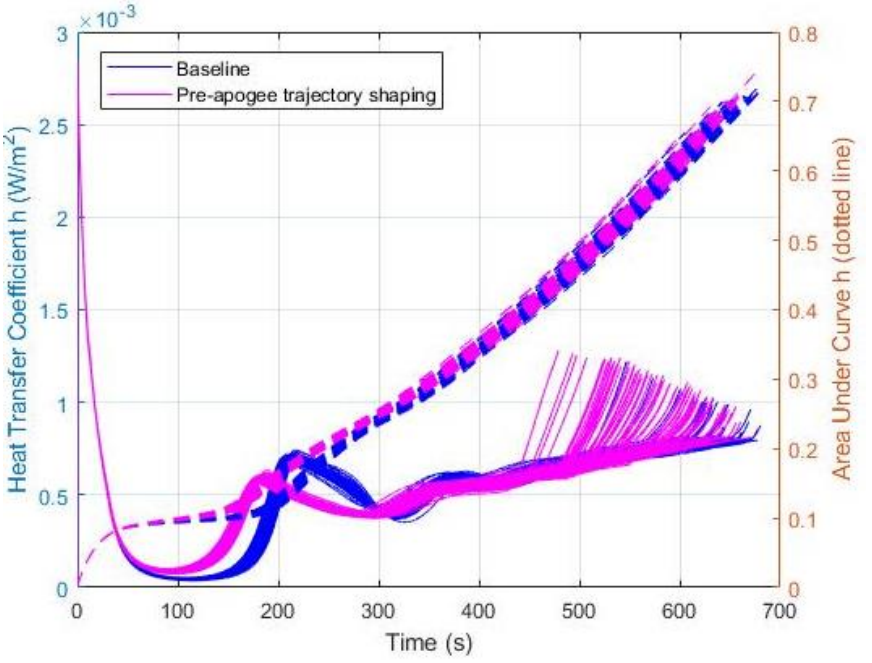

Fig. 21 Increased rocket motor terminal guidance heat transfer coefficient and area under the curve

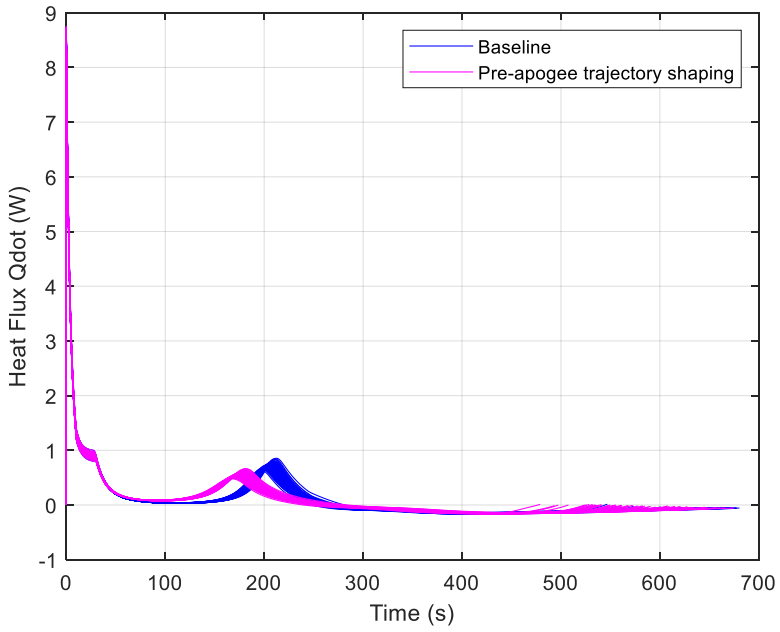

Fig. 22 Increased rocket motor terminal guidance heat flux

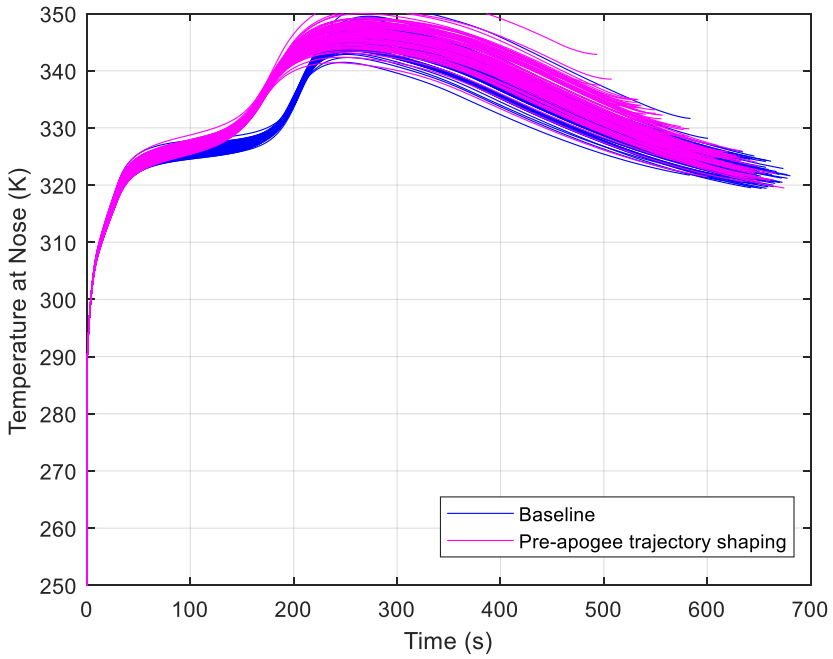

Fig. 23 Increased rocket motor terminal guidance temperature at the nose

This is a worst-case scenario in which the target is located in such a part of the phugoid motion that the baseline glide cannot guide to it. If the target location were initially known, then the initial conditions would have been changed such that terminal guidance would not fly past the target in this manner. The scenario illustrates the effect of the phugoid motion on an imperfect target location.

Figure 24 shows range error. The range error is significantly decreased from a mean of –8.857 km (standard deviation 8.120 km) to a mean of –1.171 km (standard deviation 3.831) using trajectory shaping, and the munition no longer falls short. Without trajectory shaping, more of the munitions fall short of desired range. Trajectory shaping enables more rounds to be delivered to the desired range and target. The impact velocity is shown in Fig. 25. The impact velocity is increased from a mean of 147.4 m/s (34.40 m/s standard deviation) to 230.6 m/s (57.88 m/s standard deviation). Trajectory shaping can also decrease time-of-flight. This demonstrates the effect of a worst-case, imperfectly located target on the baseline glide, which lacks the flexibility to guide-to-target during certain points of the trajectory due to the phugoid oscillation. This issue is mitigated by trajectory shaping at a quasi-equilibrium glide and shows that trajectory shaping gives flexibility for imperfectly located targets. For longer time-of-flight trajectories, the results of altered time-of-flight could prove useful. This is an area of future research. Impact velocity can be increased by using trajectory shaping and guiding to desired range.

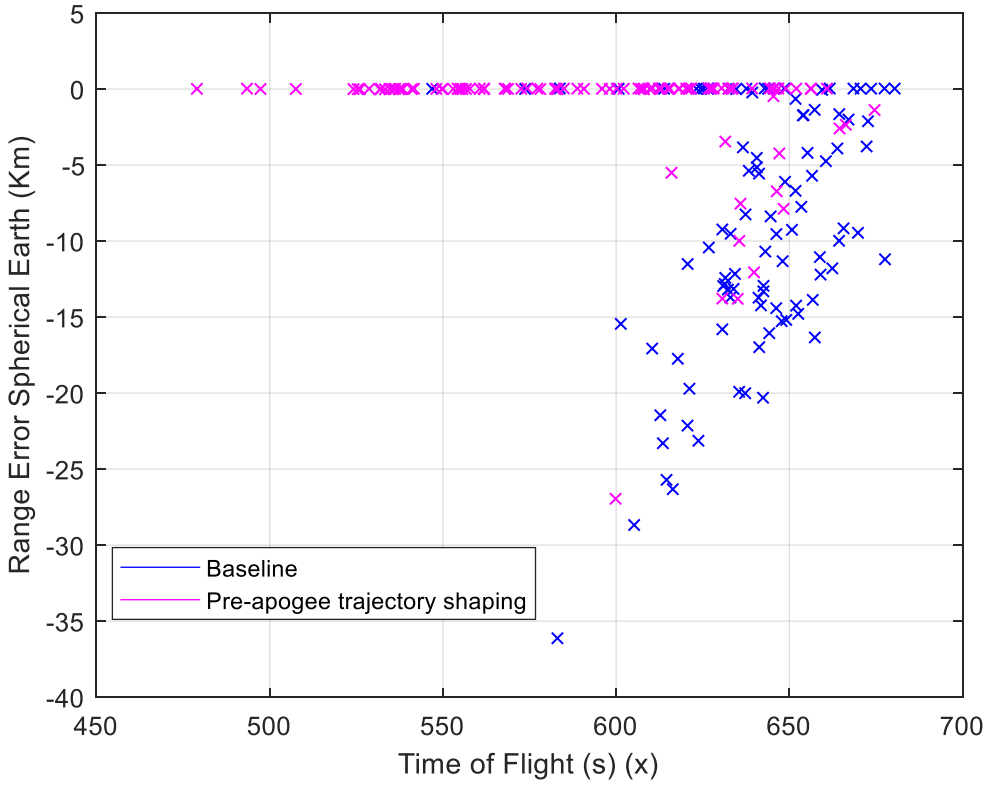

Fig. 24 Range error for a worst-case initialization in which the target is imperfectly located and the quadrant elevation is not optimized, and trajectories beyond 300 km are cut off and not plotted

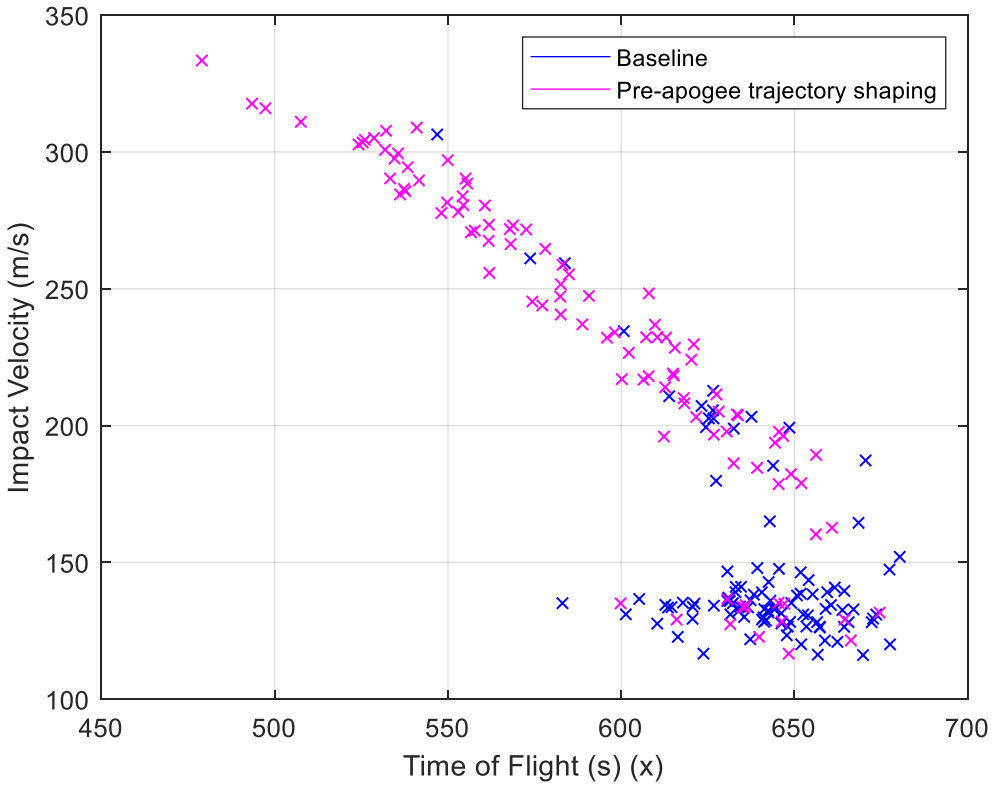

Fig. 25 Impact velocity for worst-case target placement

7. Conclusion

In this report, the phugoid motion in munitions is eliminated by gliding in a quasi-equilibrium glide. By gliding at an optimum height, range error is decreased and impact velocity is increased. Monte Carlo simulations for example scenarios are shown for maximal range and terminal guidance scenarios. Transition from glide to terminal guidance is determined using the impact point predictor incremented with a range-to-go constraint for varied atmospheric flight. The phugoid motion results in unachievable target locations. To demonstrate the ability to hit imperfectly located targets, a Monte Carlo of a specific, worst-case target placement scenario is shown. In this worst-case scenario, impact velocity is improved by 56.47%, and range error is decreased by 86.78% over baseline gliding methods. Additionally, the time-of-flight is decreased using trajectory shaping. As a result, future research will focus on allowing multiple, simultaneous munitions to be delivered from the same weapon.

8. References

Allen J, Eggers AJ. A study of the motion and aerodynamic heating of ballistic missiles entering the earth's atmosphere at high supersonic speeds. Moffett Field (CA): National Advisory Committee for Aeronautics; 1953 Apr. NACA Report No.: 1381.

Cooper G, Fresconi F, Costello M. Flight stability of an asymmetric projectile with activating canards. Journal of Spacecraft and Rockets. 2012;49(1):130–135.

Fleeman E. Missile design and system engineering. Reston (VA): American Institute of Aeronautics and Astronautics, Inc.; 2012.

Fresconi F. Guidance and control of a projectile with reduced sensor and actuator requirements. Journal of Guidance, Control and Dynamics. Nov–Dec 2011;34(6).

Fresconi FE, Celmins I, Silton S, Costello M. High maneuverability projectile flight using low cost components. Aerospace Science and Technology. 2015;41:175–188.

Hale FJ. Introduction to space flight. Upper Saddle River (NJ): Prentice Hall; 1994.

Jerger JJ. Systems preliminary design principles of guided missile designs. New York (NY): D. Van Nostrand Company, Inc.; 1960.

Lu P. Entry guidance: a unified method. Journal of Guidance, Control and Dynamics. 2014;37(3):713–728.

Lu P, Forbes S, Baldwin M. Gliding guidance of high L/D hypersonic vehicles. AIAA GN&C Conference; 2013; Boston, MA.

McCoy RL. Modern exterior ballistics: the launch and flight dynamics of symmetric projectiles. Atglen (PA): Schiffer Military History; 2012.

Ohlmeyer EJ, Phillips CA. Generalized vector explicit guidance. Journal of Guidance, Control, and Dynamics. 2006;29(2):261–268.

Strohm L. Long range precision fires: range extension study. Aberdeen Proving Ground (MD): Army Research Laboratory; 2019 forthcoming.

1 (PDF) DEFENSE TECHNICAL INFORMATION CTR DTIC OCA

1 (PDF) CCDC ARL FCDD RLD CL TECH LIB

1 (PDF) GOVT PRINTG OFC A MALHOTRA

22 (PDF) CCDC ARL FCDD RLW LE
L FAIRFAX
P WEINACHT
J BRYSON
I CELMINS
J DESPIRITO
F FRESCONI
B GRUENWALD
C MERMAGEN
G OBERLIN
J PAUL
L STROHM
J VASILE
J SAHU
FCDD RLW LF
B NELSON
T BROWN
J CONDAN
D EVERSON
M HAMAOUI
M ILG
B KLINE
D PETRICK
B TOPPER